Journal of Catalysis 263 (2009) 239–246

Contents lists available at ScienceDirect

Journal of Catalysis

www.elsevier.com/locate/jcat

Hydrodechlorination of trichloroethylene on noble metal promoted Cu-hydrotalcite-derived catalysts

N. Barrabes [a,b], D. Cornado [a,b], K. Foettinger [a,*], A. Dafinov [b], J. Llorca [c], F. Medina [b], G. Rupprechter [a]

[a] Institute of Materials Chemistry, Vienna University of Technology, Veterinärplatz 1, 1210 Vienna, Austria
[b] Department of Chemical Engineering, Rovira i Virgili University, Campus Sescelades, 43007 Tarragona, Spain
[c] Institut de Tècniques Energètiques, Universitat Politècnica de Catalunya, Diagonal 647, 08028 Barcelona, Spain

ARTICLE INFO

Article history:
Received 3 November 2008
Revised 4 February 2009
Accepted 14 February 2009
Available online 3 March 2009

Keywords:
Cu-hydrotalcites
Hydrodechlorination
Trichloroethylene
Ethylene
HRTEM
PdCu
PtCu
Alloy
Mixed oxides

ABSTRACT

Pt and Pd containing Cu-hydrotalcite-type precursors were applied as catalysts for the hydrodechlorination of trichloroethene (TCE) to ethene in gas phase. Characterization was done by XRD, TGA, TPR, HRTEM and FTIR spectroscopy of CO adsorption. High activity (>90% conversion) and excellent selectivity of more than 90% ethene were obtained at 300 °C and stoichiometric concentrations of hydrogen and TCE. The materials were synthesized by co-precipitation according to two different synthesis protocols. HRTEM measurements of the two differently prepared materials revealed fundamental differences at the microstructural level, i.e. detecting alloy formation on the samples prepared with a reduction step before Pd (Pt) introduction (alloy composition approximately $Cu_{0.4}Pt_{0.6}$ and $Cu_{0.25}Pd_{0.75}$), whereas no alloy formation was observed on the samples prepared without the previous reduction step during synthesis. Whereas the former alloyed catalysts were stable during the reaction, the latter catalysts exhibited decreasing rate of ethene formation with time on stream due to increasing Cu areas blocked by Cl, which can be explained by a less effective regeneration and less availability of hydrogen due to the worse contact between noble metal and Cu (separate noble metal and Cu particles). We propose that the reaction proceeds via cleavage of the C–Cl bond on Cu, which is then regenerated by spillover of hydrogen from the noble metal.

1. Introduction

Chlorinated organic compounds are widely distributed pollutants due to their extensive use for metal degreasing or textile cleaning, leading to the contamination of soil and groundwater. The emission of chlorocompounds into the environment is now strictly regulated, due to the severe influence on health and ecological damage. The decomposition of hazardous chlorinated waste by incineration is highly energy demanding, and incomplete combustion can lead to the release of toxic heterocyclic organic compounds. For this reason catalytic hydrodechlorination is gaining importance as an alternative low-energy, non-destructive method, which enables the conversion of industrial by-products to valuable chemical feedstock or environmentally friendly products.

Noble metals are very active for the hydrodechlorination of chlorinated organic compounds producing fully hydrogenated products [1,2]. The dechlorination of trichloroethene (TCE) on noble metal catalysts may follow a mechanism similar to the one proposed by Ordónez et al. [3] where the double bond hydrogenation occurs catalytically, while the elimination of HCl is essentially non-catalytic. Ethylene is then quickly hydrogenated on the surface of a very active hydrogenation catalyst such as Pd [1]. The modification of supported Pt or Pd catalysts by addition of a second metal dramatically changes the catalytic performance with respect to vicinal chlorocarbon dechlorination; the catalysts become highly selective toward olefins [4,5]. A number of transition metal additives were investigated with the best performance observed for Pt–Cu [5,6], Pt–Sn [7] and Pd–Ag [8] combinations. Kovalchuk and d'Itri [5] proposed that the governing factor for the high olefin selectivity of bimetallic catalysts in hydrogen-assisted dechlorination of chlorocarbons is the low adsorption energy for olefins on active sites, which consist of isolated noble metal atoms in a matrix of the modified catalyst's surface. However, the mechanistic details of this phenomenon are still under investigation.

Deactivation is a main problem of monometallic catalysts. Some recent examples were reported in [9–11]. Bimetallic catalysts deactivate less with time on stream. In the literature different explanations are suggested for the deactivation of the catalysts in gas-phase hydrodechlorination. Poisoning of the active sites by HCl, produced during the reaction, was proposed as main cause for deactivation by many authors [3,12–15]. Other works reported that poisoning by HCl is of minor importance for noble metals and suggest metal particle sintering and coke deposition as main

* Corresponding author. Fax: +43 1 25077 3890.
E-mail address: kfoettinger@imc.tuwien.ac.at (K. Foettinger).

0021-9517/$ – see front matter
doi:10.1016/j.jcat.2009.02.015

causes for deactivation [14,16]. In addition, HCl can increase the surface acidity of inorganic supports, such as alumina, by forming Al-chlorides, which are strong Lewis acids that may favor the formation of carbonaceous deposits on the catalyst surface [17].

Transition metal containing hydrotalcites (HT), particularly copper-containing hydrotalcites are receiving increasing attention due to their diverse applications in catalysis [18–20]. Hydrotalcite-type compounds possess two-dimensional layered structures with alternating positively charged mixed metal hydroxide sheets and negatively charged interlayer anions along with water molecules. Their structure can be deduced from the brucite lattice $\{Mg(OH)_2\}$ with partial replacement of Mg^{2+} by a trivalent cation like Al^{3+}. The resulting excess positive charge is compensated by anions, usually carbonate, occupying interlayer positions. Alejandre et al. [21,22] demonstrated that copper ions can be incorporated partially or totally as divalent cations in the layered structure of the HT. Then after calcination high dispersion of the metal oxide phase is obtained. Furthermore, it has been demonstrated that the basic properties of these materials play an important role in the activity and stability for hydrodechlorination of trichlorobenzene [23]. Therefore, they could potentially become interesting new catalysts for hydrodechlorination processes.

The aim of this work was to investigate the catalytic properties of catalysts prepared from hydrotalcite-like materials containing Cu and Mg, as well as the effect of the addition of noble metals like Pt and Pd for the gas-phase hydrodechlorination of trichloroethylene (TCE), in order to improve the catalyst stability and selectivity to ethene. By changing the preparation procedure and the interaction between Cu and noble metal a different catalytic behavior has been observed and studied in detail.

2. Experimental

2.1. Catalyst synthesis

MgCuAl hydrotalcites were prepared by a standard co-precipitation procedure combining a solution of $Mg(NO_3)_2{\cdot}6H_2O$, $Al(NO_3)_3{\cdot}9H_2O$ and $Cu(NO_3)_2{\cdot}5H_2O$ in adequate amounts, with a second solution containing NaOH as precipitating agent.

At room temperature, both solutions were slowly and simultaneously added to a beaker containing distilled water under vigorous stirring, at a pH value around 9–10. The resulting suspension was then kept at 25 °C with further stirring for 18 h. The resulting solid was filtered and washed several times with distilled water and dried at 100 °C for 2 h. The hydrotalcite was calcined at 450 °C overnight obtaining a Cu/Mg/Al mixed oxide. For the incorporation of the noble metals two different protocols were applied.

In the first protocol (labeled as "-R") the materials were reduced under hydrogen for 3 h at 350 °C. After reduction, the sample was introduced into an aqueous solution containing the palladium or platinum nitrate salts under stirring at room temperature. All steps were carried out under argon atmosphere in order to avoid reoxidation of copper. The noble metal solution had been degassed by bubbling with argon for 1 h before adding the reduced Cu-HT sample. In this step the palladium and platinum is reduced by a redox process with copper and deposited on the surface of the catalyst. Then the solid was filtered and dried at 100 °C. Finally, calcination was performed for 2 h at 300 °C. A new reduction process was carried out in a hydrogen flow of 14 ml/min for 30 min at 300 °C prior to the reaction.

The second synthesis protocol was followed (and labeled as "-WR"), omitting the reduction step before the noble metal introduction. The calcined material was impregnated with an aqueous solution of the noble metal salts. Then the solid was dried at 100 °C, followed by calcination and reduction as in the first protocol.

Table 1a
Overview of the hydrotalcite materials used in this work.

Label	Molar ratio (Cu + Mg)/Al	Molar ratio Cu/Mg
$Mg_1Cu_2Al_1$	≅3	≅2
$Mg_{1.5}Cu_{1.5}Al_1$	≅3	≅1
$Mg_2Cu_1Al_1$	≅3	≅0.5

Nominal composition according to the amounts applied in the syntheses.

Table 1b
Overview of the noble metal promoted catalysts.

Label	Pd (Pt) loading (wt%)	Preparation procedure
Pd (Pt)-$Mg_1Cu_2Al_1$-R	0.5	Protocol 1
Pd (Pt)-$Mg_{1.5}Cu_{1.5}Al_1$-R	0.5	Protocol 1
Pd (Pt)-$Mg_2Cu_1Al_1$-R	0.5	Protocol 1
Pd (Pt)-$Mg_{1.5}Cu_{1.5}Al_1$-WR	0.5	Protocol 2

The obtained materials used in this study are compiled in Tables 1a and 1b.

2.2. Characterization

Cu-hydrotalcites without calcination were analyzed by thermogravimetric measurements (TG) on a Netzsch STA 409 PC/4/H Luxx apparatus in nitrogen flow applying a heating rate of 10°/min.

Powder X-ray diffraction patterns of the different samples were obtained on a Siemens D5000 diffractometer using nickel-filtered Cu Kα radiation. The patterns were recorded over a range of 2θ angles from 10° to 90° and crystalline phases were identified using the Joint Committee on Powder Diffraction Standards (JCPDS) files.

Temperature-programmed reduction (TPR) studies of the samples were performed using a TPD/R/O 1100 (ThermoFinnigan) equipped with a thermal conductivity detector (TCD) and coupled to a mass spectrometer QMS 422 Omnistar. Before reduction, the sample (around 100 mg) was dried under flowing helium at 120 °C for 24 h. The reduction was carried out between room temperature and 800 °C at a heating rate of 10 °C/min flowing a gas mixture of 5% H_2 in argon (20 ml/min total flow). Peak deconvolution was done with the software Suite for TPD/R/O 1100 (ThermoQuest).

The Fourier transform infrared (FT-IR) spectra were recorded on a Bruker IFS 28 spectrometer equipped with an MCT detector at a resolution of 4 cm^{-1}. The measurement cell is connected to a vacuum system working in the 10^{-6} mbar range and allows in situ pre-treatments of samples. The catalysts were pressed into self-supporting wafers and were reduced in 500 mbar of pure H_2 at 300 °C. After keeping the catalyst in hydrogen atmosphere at that temperature for 30 min, the cell was evacuated for another 30 min at the reduction temperature. CO adsorption measurements were carried out at 20 °C using 5 mbar of pure CO, followed by evacuation of the gas phase CO at 20 °C.

High-resolution transmission electron microscopy (HRTEM) was carried out with a JEOL 2010F instrument equipped with a field emission source. The point-to-point resolution was 0.19 nm and the resolution between lines was 0.14 nm. Samples were grounded and deposited on holey-carbon-coated grids from ultrasonicated alcohol suspensions. About 200–250 individual particles were used in each sample for particle size determination.

2.3. Catalytic activity

The catalysts were tested for the hydrodechlorination reaction of trichloroethene (TCE) using a continuous fixed-bed glass reactor at 100–300 °C and atmospheric pressure. For all experiments 0.1 g catalyst were used. The gas feed is obtained by flowing an inert gas (He) and hydrogen through a saturator kept at 25 °C, containing trichloroethylene (TCE) in liquid phase, which results in a TCE

partial pressure of 92 mbar. Two different molar ratios of H_2:TCE were employed in this study, 2:1 (substoichiometric) and 3:1 (stoichiometric). The gas flows are adjusted by mass flow controllers (Brooks Instrument 0154) and introduced into the reactor, which is placed in a furnace coupled with a temperature controlling system. The outlet of the reactor is connected by a six-way valve to a gas chromatograph (HP 5890 series II, HP Poraplot column, FID). Quantification was done by analyzing the peak areas of TCE, ethane and ethene, the amount of formed hydrogen chloride was not quantified in our experiments.

3. Results and discussion

3.1. Characterization of the catalysts

Thermogravimetric analyses of the uncalcined samples were carried out in flowing nitrogen. For hydrotalcite-like materials, usually two or three mass steps due to (1) dehydration, (2) layer dehydroxylation, and (3) anion decomposition are observed [21]. Similar results are obtained for all the samples. Two main weight losses that are in agreement with previous works [19,24,25] are observed (not shown). The first weight loss occurs between 100 °C and 200 °C and corresponds to the dehydration through removal of water in the interlayer space of the hydrotalcite as well as some adsorbed water. The second weight loss between 220 °C and 500 °C is attributed to dehydroxylation of the brucite-like layers and decomposition of the anions located in the interlayer space. A decrease of the Cu^{2+} content in the brucite-like layers produces a slight increase of the dehydroxylation and decomposition temperature of the MgCuAl hydrotalcites. This behavior was also observed by Kannan et al. [19] and was explained by the better stabilization of Mg^{2+} in the octahedral coordination of the HT lattice compared to copper.

Powder X-ray diffraction patterns were recorded of HTs before and after calcination. The uncalcined hydrotalcite samples show the typical diffraction lines of the HT-like phase without any additional peaks corresponding to other crystalline phases. The X-ray diffraction patterns of all samples are nearly identical, which can be explained by the small difference in the octahedral ionic radii of Cu^{2+} (0.73 Å) and Mg^{2+} (0.72 Å) [26]. After calcination at 450 °C the hydrotalcite phase disappears leading to formation of the tenorite phase (CuO) in agreement with previous works [25,27]. The noble metal containing materials exhibit the same XRD patterns. Diffraction patterns corresponding to Pt or Pd are not observed due to the small loading and good dispersion (observed by HRTEM, see later).

The results of the temperature-programmed reduction (TPR) of the calcined Cu–Mg–Al mixed oxides ("Cu-HT") and a corresponding Pt-containing sample (Pt-$Mg_{1.5}Cu_{1.5}Al_1$-R) are displayed in Fig. 1. The Cu-HT samples show a broad peak around 300 °C, which can be split into two components around 260 °C and 320 °C, respectively. The first peak is attributed to the reduction of the highly dispersed copper oxide species, which include isolated copper cations and small two- or three-dimensional clusters [28]. The second peak around 320 °C may be assigned to the reduction of large bulk-like CuO particles to Cu^0, formed during the calcination process [21]. Reduction for all HT-samples is practically completed at a temperature below 400 °C. With the gradual replacement of magnesium with copper cations, the first reduction peak decreases. After peak deconvolution we estimate that about 70% of the total hydrogen consumption can be attributed to the feature at 320 °C on $Mg_1Cu_2Al_1$, whereas this fraction decreases to 60% for the $Mg_{1.5}Cu_{1.5}Al_1$ sample. This indicates a higher dispersion of the CuO phase with increasing Mg content and therefore a higher portion of easily reducible copper particles [25].

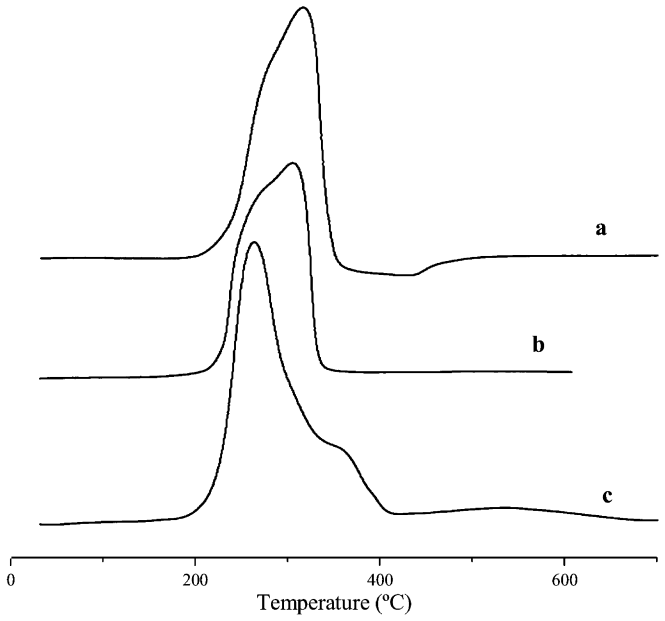

Fig. 1. Temperature-programmed reduction profiles of Cu-HT and Pt-Cu-HT catalysts: (a) $Mg_1Cu_2Al_1$; (b) $Mg_{1.5}Cu_{1.5}Al_1$ and (c) 0.5% Pt-$Mg_{1.5}Cu_{1.5}Al_1$-R.

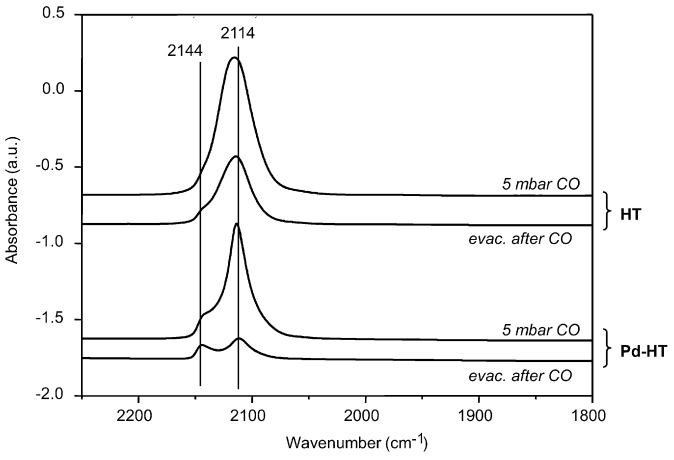

Fig. 2. FTIR spectra of CO adsorption at 20 °C in the presence of 5 mbar CO background pressure followed by evacuation at 20 °C on $Mg_2Cu_1Al_1$ and Pd-$Mg_2Cu_1Al_1$-R.

When the noble metal is introduced, the CuO reduction is facilitated resulting in an increase of a reduction peak at lower temperature. CuO that is in close contact with Pt is reduced at lower temperatures, whereas a shoulder around 350 °C is attributed to the reduction of CuO isolated from Pt particles. We expect the presence of significant amounts of such isolated copper particles due to the fact that Cu is in large excess. Such "isolated" species would thus be reduced at higher temperatures.

Practically the same TPR profiles were observed on the samples containing Pd (not shown in Fig. 1).

FT-IR spectroscopy of CO adsorption was used to obtain information about the state of the noble metal particles and copper species on the surface. Fig. 2 shows a comparison of the spectra after CO adsorption on $Mg_2Cu_1Al_1$ and Pd-$Mg_2Cu_1Al_1$-R catalysts. In the presence of 5 mbar CO background pressure the main CO band appears at around 2114 cm^{-1} on all samples, with a small shoulder at higher frequencies at approximately 2144 cm^{-1}. After evacuation of the CO gas phase at room temperature the intensity

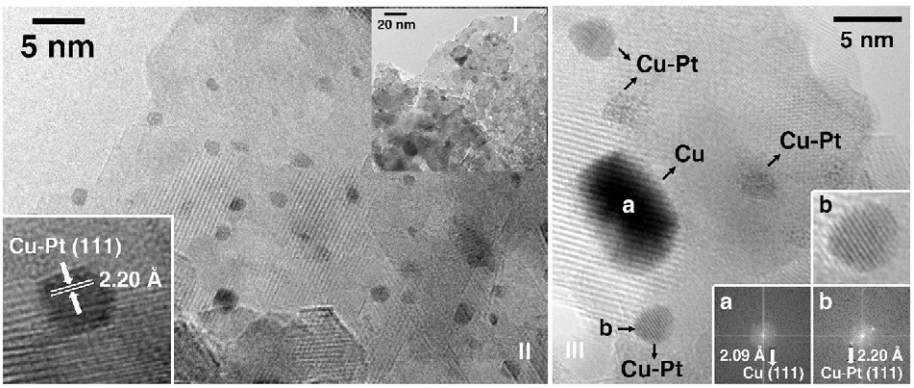

Fig. 3. HRTEM image of 0.5% Pt-$Mg_{1.5}Cu_{1.5}Al_1$-R.

of the band at 2114 cm^{-1} decreases strongly, whereas the high frequency band at 2144 cm^{-1} remains constant in intensity.

For the $Mg_2Cu_1Al_1$ catalyst, the band at 2144 cm^{-1} is assigned to CO adsorbed on Cu^+. This assignment is supported by the stability of this band at room temperature evacuation. When considering the frequency ranges reported in literature [29] the band at 2114 cm^{-1} could be attributed to CO linearly bonded on Cu^+ or on metallic Cu^0.

Bands of CO adsorbed on copper in different oxidation states are not straightforward to identify and distinguish. Cu^{2+} is difficult to detect by CO adsorption, because it can easily get reduced by CO. Besides, CO–Cu^{2+} is a very weak interaction occurring typically at low temperatures and high pressures [29]. For CO adsorbed on Cu^+ the appearance of a high-frequency and a low-frequency band was reported at around 2160–2145 and 2130–2115 cm^{-1} [29,30], with the latter being less stable, which is very similar to our results. Discrimination of CO on Cu^0 and Cu^+ is possible via the different stability of the bands and via regarding the coverage-dependence of the band position. The frequency of νCO on Cu^+ is not or only weakly coverage-dependent in contrast to CO on Cu^0 [29]. In our measurements the intensity of the band at 2114 cm^{-1} decreases after evacuation. The addition of Pd in the sample Pd-$Mg_2Cu_1Al_1$-R results in a stronger decrease in the intensity of the band at 2114 cm^{-1} upon evacuation whereas the band at 2144 cm^{-1} remained constant (see Fig. 5). By TPR we have observed that the addition of Pd shifts the reduction of copper to lower temperature. It is known that CO is strongly adsorbed on Cu^+ ions since the carbonyls formed are stabilized by π-backdonation that is not performed on Cu^0 due to the high electron density. The introduction of Pd increases the electron density of the metal phase weakening the CO–metal bond. Based on this, the two bands at 2114 and 2144 cm^{-1} can most likely be assigned to Cu^0–CO and Cu^+–CO species, respectively.

Bands of CO adsorbed linearly on Pd^0 or $Pd^{\delta+}$ are most probably masked by bands of CO on Cu^0 or Cu^+ due to the large excess of copper. The same holds for the 0.5% Pt on HT samples. However, no vibrational bands due to CO bridge-bonded on zerovalent Pd in the range 2000–1895 cm^{-1} or CO adsorbed in 3-fold hollow sites on Pd in the range 1920–1830 cm^{-1} were observed. This could either indicate a good noble metal dispersion and a minor contribution of Pd atoms situated in crystal planes on the small metal clusters (which were detected by HRTEM, see the following section), or hint to alloy formation and thus dilution of larger Pd ensembles. However, another possible explanation could be a detectability problem as possible reason for the absence of CO in bridge and hollow sites.

The CO-FTIR study was also performed on the Pt containing samples. Similar spectra as on the Pd promoted materials were obtained and thus no additional information could be gained.

Beside the CO stretching vibration bands, broad bands in the range of 3700–2900 cm^{-1} due to residual water were observed as well as bands below 1670 cm^{-1}, which can be attributed to carbonate-type species.

The samples 0.5% Pt and 0.5% Pd on $Mg_{1.5}Cu_{1.5}Al_1$-R were analyzed by HRTEM in order to study the distribution, size and state of the metallic particles. Fig. 3(I) shows a bright field, low magnification image of the 0.5% Pt-$Mg_{1.5}Cu_{1.5}Al_1$-R sample. It is mostly constituted by small, well-dispersed particles less than 2 nm in diameter. In order to get insight into their composition, numerous images were taken under high resolution mode (HRTEM). A representative HRTEM image is shown in Fig. 3(II). A careful examination of this figure indicates that particles with diameters between 1 and 2 nm and exhibiting higher contrast are located at the borders of substrate crystallites, being the mean particle size of the particles centered at ca. 1.4 nm. An enlargement of one of these particles oriented along a crystallographic axis (see inset of Fig. 3(II)) shows lattice fringes at 2.20 Å. Taking into account that metallic copper exhibits (111) spacings at 2.088 Å whereas the (111) planes of Pt metal are located at 2.265 Å, and that copper and platinum form solid solutions, the lattice fringes at 2.20 Å detected in this sample are indicative of solid solution formation between Cu and Pt. From the Vegard's law, $a_{alloy} = xa_{Pt} + (1-x)a_{Cu}$, a value of $x = 0.6$ is deduced from $a_{alloy} = 3.803$ Å (obtained from lattice fringes at 2.20 Å and assuming (111) crystallographic planes), thus meaning that the composition of Cu–Pt nanoparticles in these catalysts is approximately $Cu_{0.4}Pt_{0.6}$. Fig. 3(III) shows another HRTEM image for this sample. Several Cu–Pt alloy particles are recognized. An analysis of particle labeled "b" in the image (see insets in direct mode and Fourier transform images) reveals the presence of lattice fringes again at 2.20 Å, corresponding to (111) planes of the alloy. In addition to Cu–Pt alloy nanoparticles, the sample also contains other particles of about 8–10 nm in diameter which correspond to pure Cu. As an example, particle labeled "a" in Fig. 3(III) corresponds to one of these Cu metal particles, identified by the presence of spots at 2.09 Å in the corresponding Fourier transform image (see inset), which are ascribed to (111) crystallographic planes of metallic Cu. Therefore, this sample is mainly constituted by Cu–Pt alloy nanoparticles of 1–2 nm in size with approximate composition $Cu_{0.4}Pt_{0.6}$ and by larger Cu particles of 8–10 nm.

Fig. 4(I) shows a low-magnification image of 0.5% Pd-$Mg_{1.5}Cu_{1.5}Al_1$-R. Particles of about 1–5 nm are very well dispersed over the support, being the mean particle size of about 2.6 nm. The characterization of individual particles was accomplished by HRTEM analysis. Fig. 4(II) corresponds to a representative HRTEM image. Particle labeled "a", with a diameter of ca. 5 nm, exhibits lattice fringes at 2.21 Å (see the Fourier transform image in the corresponding inset). Exactly the same lattice fringes at 2.21 Å are recognized in particle labeled "b" (see inset), which

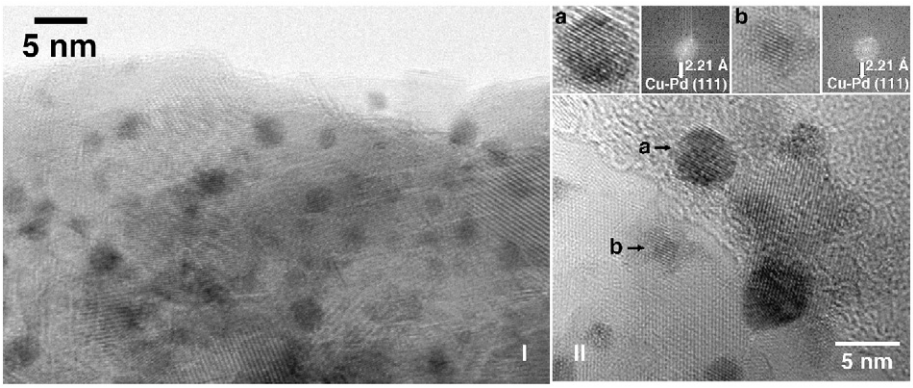

Fig. 4. HRTEM image of 0.5% Pd-$Mg_{1.5}Cu_{1.5}Al_1$-R.

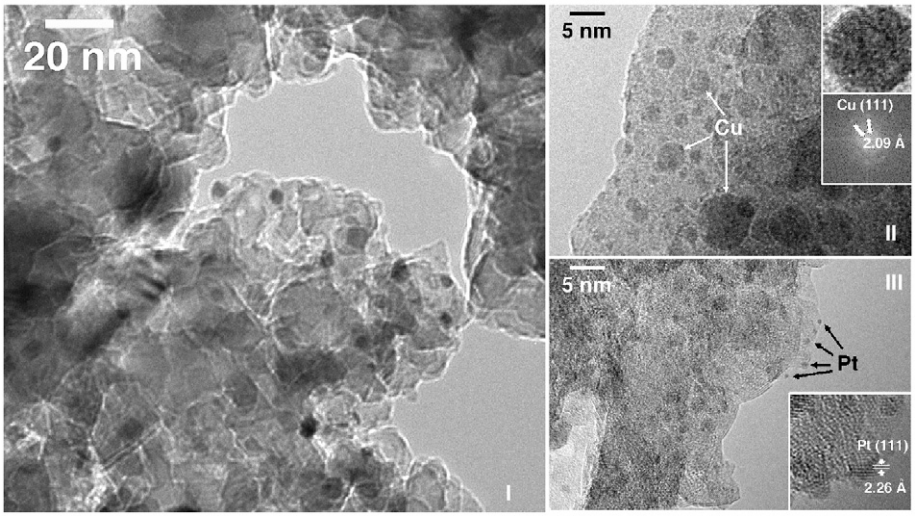

Fig. 5. HRTEM image of 0.5% Pt-$Mg_{1.5}Cu_{1.5}Al_1$-WR.

is much smaller, about 1.5 nm in diameter. Lattice-fringe images recorded through different parts of this sample yields similar values (2.21 ± 0.01 Å). Assuming (111) planes, a lattice fringe of 2.21 Å implies a cell parameter of $a_{alloy} = 3.824$ Å. From Vegard's law for the Cu–Pd system, this cell parameter corresponds to an alloy composition of ca. $Cu_{0.25}Pd_{0.75}$.

Furthermore we performed a TEM study of the materials obtained according to the modified synthesis protocol, without reduction of the calcined Cu-HT before impregnation with the respective (Pt, Pd) noble metal. Following this protocol we expected to avoid alloy formation and to obtain worse noble metal dispersion. These samples (0.5% Pt-$Mg_{1.5}Cu_{1.5}Al_1$-WR and 0.5% Pd-$Mg_{1.5}Cu_{1.5}Al_1$-WR) were analyzed by HRTEM in order to confirm the hypothesis. The sample not reduced before Pt incorporation is different at the microstructural level from the sample discussed above, which was reduced before Pt impregnation. Fig. 5(I) shows a general view of this sample in bright-field mode. Apparently, well-distributed particles of about 4–8 nm in diameter are present throughout the entire sample. A close examination by HRTEM, however, reveals that the sample is in fact constituted by particles ranging from 0.8 to 10 nm in diameter. A representative example of this degree of particle dimensions is given in Fig. 5(II). Lattice-fringe analysis of individual particles performed by HRTEM suggests that larger particles correspond to metallic Cu, whereas the smallest particles can be identified with Pt nanoparticles. Insets in Fig. 5(II) show an enlargement of one of the big particles along with its Fourier transform image. Spots at 2.09 Å are indicative of (111) crystallographic planes of metallic Cu. On the other hand, Fig. 5(III) shows small Pt particles, which are marked by arrows. The lattice fringes at 2.26 Å shown in the inset of Fig. 5(III) are ascribed to (111) planes of Pt metal. Although the presence of alloy particles in this sample cannot be completely ruled out, it appears from HRTEM analysis that the sample is mainly comprised by separate Cu and Pt entities.

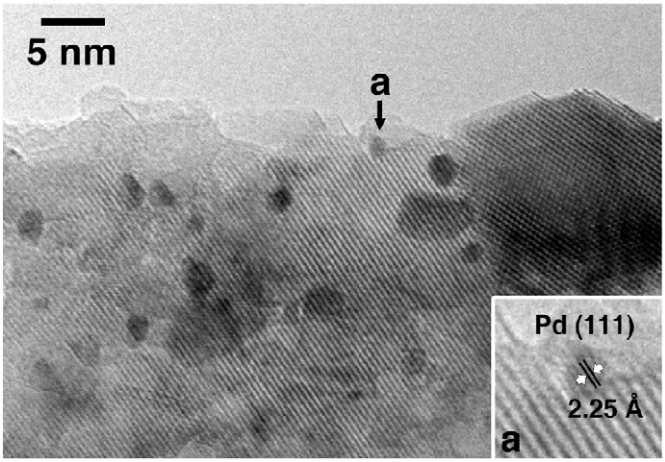

Fig. 6. HRTEM image of 0.5% Pd-$Mg_{1.5}Cu_{1.5}Al_1$-WR.

A general view of the 0.5% Pd-$Mg_{1.5}Cu_{1.5}Al_1$-WR sample is depicted in Fig. 6. Particles ranging from 1 to 15 nm are distributed along the sample. In a similar way to that observed for the sample

Table 2
Influence of the catalyst composition on conversion and selectivity (reaction conditions: 300 °C; molar ratio H_2:TCE = 2:1).

Catalyst	Conversion (%)	Ethylene selectivity (%)	Rate ($\mu mol\, g^{-1}\, cat.\, s^{-1}$)
0.5% Pd-$Mg_1Cu_2Al_1$-R	22	97	6.83 ± 0.10
0.5% Pd-$Mg_{1.5}Cu_{1.5}Al_1$-R	14	98	4.34 ± 0.07
0.5% Pd-$Mg_2Cu_1Al_1$-R	29	96	9.00 ± 0.13
0.5% Pt-$Mg_1Cu_2Al_1$-R	30	92	9.31 ± 0.14
0.5% Pt-$Mg_{1.5}Cu_{1.5}Al_1$-R	25	93	7.76 ± 0.12
0.5% Pt-$Mg_2Cu_1Al_1$-R	21	93	6.52 ± 0.10

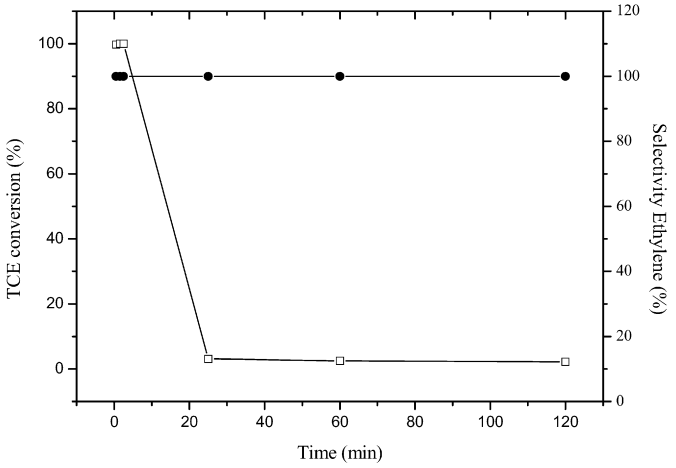

Fig. 7. Conversion and selectivity to ethene versus time on stream on $Mg_{1.5}Cu_{1.5}Al_1$ without noble metal promotion at 300 °C and stoichiometric hydrogen concentration (molar ratio H_2:TCE = 3:1). (□, Conversion of TCE; ●, ethylene selectivity.)

0.5% Pt-$Mg_{1.5}Cu_{1.5}Al_1$-WR, which was similarly prepared (no reduction step prior to noble metal incorporation), this sample contains separate Cu and Pd particles. As an example, the inset in Fig. 6 shows an enlargement of particle labeled "a", which measures ca. 2 nm in diameter. Lattice fringes at 2.25 Å are ascribed to (111) planes of metallic Pd (nominal value 2.246 Å). No Cu–Pd alloy particles have been identified by HRTEM (but their presence cannot be completely excluded due to statistical limitation of the technique).

3.2. Catalytic activity

3.2.1. Influence of the composition

The catalysts prepared from hydrotalcites with different Mg/Cu ratios ($Mg_1Cu_2Al_1$, $Mg_{1.5}Cu_{1.5}Al_1$ and $Mg_2Cu_1Al_1$) and impregnated with 0.5 wt% of Pd or Pt (-R samples) were tested in the hydrodechlorination of trichloroethylene (TCE) in a temperature range between 100 °C and 300 °C. The results obtained at 300 °C are summarized in Table 2. No clear trend is observed for the influence of the Mg/Cu ratio in the hydrotalcite precursor on activity and selectivity. 0.5 wt% Pd-$Mg_2Cu_1Al_1$-R and 0.5 wt% Pt-$Mg_1Cu_2Al_1$-R exhibited a slightly higher activity than the other samples.

Note that the ethene selectivity in Table 2 was calculated by considering only the amounts of ethene and ethane formed. Formation of 1,1-dichloroethylene, cis-1,2-dichloroethylene, trans-1,2-dichloroethylene, chloroethylene and chloroethane were also observed during the reaction but only in very small amounts (selectivity <1%).

Without noble metal promotion a very fast deactivation was observed (see Fig. 7), starting from an initial conversion of ~100% the material deactivated rapidly to approximately 2% conversion within the first minutes reaction time. Ethene was formed as the only product. According to Fung and Sinfelt [31], who studied a variety of metal catalysts for methyl chloride hydrogenolysis, the activity of Au and Ag catalysts can be explained by the ability of group IB metals to form a metal–chlorine bond, which provides a driving force for the cleavage of the C–Cl bond. Therefore, the fast deactivation of the catalyst is most probably due to Cl poisoning of the Cu sites.

Stable catalytic performance can be achieved by noble metal addition. Hardly any influence was observed with respect to the nature of the noble metal (Table 2). Similar activities were found for Pt and Pd-promoted samples, with Pd containing materials exhibiting slightly higher ethene concentrations compared to Pt-HT ones. The catalytic performance of Pt and Pd catalysts for hydrodechlorination depends on the reactants. Differences in selectivity and stability have often been observed. For some reactions Pd shows a superior performance, e.g. hydrodechlorination of CFCs to HFCs [32,33], while there are other examples where Pt catalysts show better results, i.e. gas phase hydrodechlorination of carbon tetrachloride to chloroform [32,34]. As an explanation it was suggested [32] that Pt has a more noble character than Pd and thus certain reactants or intermediates are more weakly bound on Pt. In our study we did not observe any significant differences between the two metals.

Lambert et al. [4] showed that pure copper samples exhibit a very low activity at different temperatures for 1,2-dichloroethane hydrogen-assisted dechlorination toward ethene. Chlorine atoms on the surface cannot be easily removed due to a lack of surface hydrogen. The role of the noble metal could, therefore, be to provide a sufficient supply of dissociated hydrogen for reduction of surface Cu–Cl_x species and formation of HCl, as it has been suggested by Vadlamannati et al. [35] for hydrogen-assisted dechlorination of 1,2-dichloroethane over Pt–Cu/C catalysts. Also the fact that the nature of the noble metal component does not influence the catalytic performance supports the idea that it is mainly needed for hydrogen activation regenerating the catalytic activity.

Since copper is present in large excess, it is very likely that a significant amount Cu particles not interacting with the noble metal are present, which was confirmed by HRTEM measurements. However, we assume that these isolated copper particles separated from Pd (Pt) get poisoned by Cl very fast, similar to the Cu-HT without noble metal. This means fast deactivation and therefore only minor contribution to the overall catalyst performance after a certain time on stream.

3.2.2. Influence of the preparation procedure

Two different catalyst preparation procedures had been applied (-R and -WR, see Section 2) with the aim to obtain catalysts possessing a different degree of interaction with the Cu phase. This was investigated and confirmed by means of HRTEM measurements (see Section 3.1).

The materials prepared according to these two synthesis pathways were compared with respect to their catalytic properties.

Fig. 8 shows the catalytic activity and ethene selectivity with time on stream obtained on 0.5 wt% Pd-$Mg_1Cu_2Al_1$-R and 0.5 wt% Pt-$Mg_1Cu_2Al_1$-R at 300 °C and substoichiometric hydrogen concentration (molar ratio H_2:TCE = 2:1). Both catalysts showed stable activity and selectivity for around 130 min time on stream. A slightly higher activity and selectivity to ethane was observed

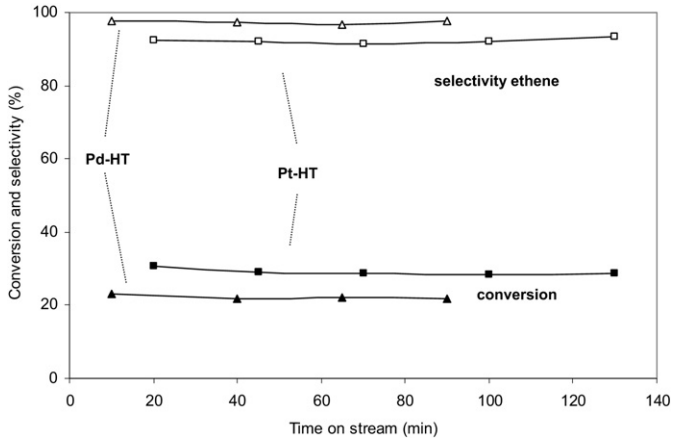

Fig. 8. Conversion and selectivity to ethene versus time on stream on Pd- and Pt-$Mg_1Cu_2Al_1$-R at 300 °C and substoichiometric hydrogen concentration (molar ratio H_2:TCE = 2:1). (▲, ■, Conversion of TCE; △, □, ethene selectivity; triangles represent Pd-HT and squares Pt-HT catalysts.)

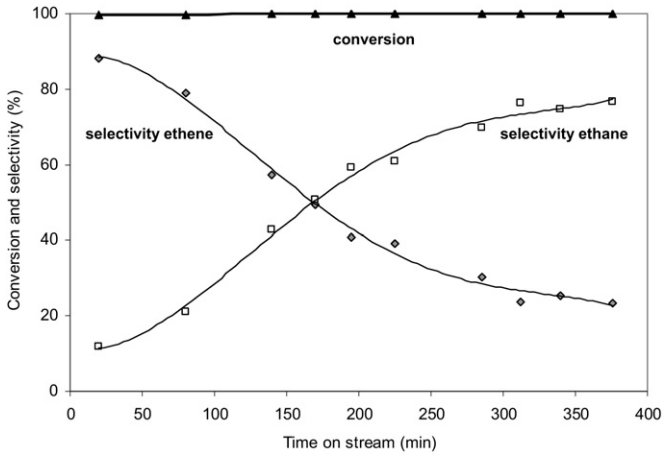

Fig. 9. Catalytic activity and selectivities obtained on 0.5% Pd-$Mg_{1.5}Cu_{1.5}Al_1$-WR at 300 °C under stoichiometric conditions (molar ratio H_2:TCE = 3:1). (▲, TCE conversion; □, ethane selectivity; ◆, ethene selectivity.)

Table 3
Effect of the H_2:TCE molar ratio (300 °C; 0.5% Pt-$Mg_{1.5}Cu_{1.5}Al_1$-R).

H_2:TCE	Conversion (%)	Ethylene selectivity (%)
Substoichiometric 2:1	24	94
Stoichiometric 3:1	98	94

for the Pd catalysts with respect to Pt ones. However, in both cases, the selectivity to ethene was higher than 95% during time on stream.

When the H_2:TCE molar ratio is increased to 3:1, i.e. stoichiometric conditions, the conversion increases from 24% up to nearly total conversion (98%), as can be seen in Table 3 for the 0.5% Pt-$Mg_{1.5}Cu_{1.5}Al_1$-R catalyst. However, the selectivity to ethene remained practically constant (94%). This can be explained because at a higher hydrogen concentration, the chloride species bound to the copper are removed to a larger extent, leading to reactivation of copper active sites, without changing the catalytic behavior.

However, when the catalyst was prepared using the second synthesis protocol the performance at the same reaction conditions was different. The 0.5% Pd-$Mg_{1.5}Cu_{1.5}Al_1$-WR catalyst showed a total conversion of TCE at 300 °C and at a H_2:TCE molar ratio 3:1 (see Fig. 9). Constant activity is observed with time on stream, whereas the selectivity decreases. At the beginning of the reaction the main product was ethene with a selectivity around 90% and a selectivity to ethane of around 10%. During time on stream the selectivity to ethene decreases at the same time that the selectivity to ethane increases. After around 380 min time on stream the selectivity to ethene was around 20% whereas the selectivity to ethane increased up to 80%. The different catalytic behavior obtained for the catalysts prepared by the two different protocols could be explained considering a different interaction between the noble metal (Pt or Pd) and Cu. From HRTEM measurements we have observed alloy formation between noble metal and Cu using the first protocol synthesis whereas using the second protocol the sample is mainly comprised by separate Cu and noble metal entities.

Based on the results presented so far we suggest a reaction scheme similar to what was proposed by the groups of Heinrichs [36] and d'Itri [6] for hydrogen-assisted dechlorination of dichloroethane on bimetallic catalysts. The different catalytic behavior observed on Pt- or Pd-Cu-hydrotalcite catalysts using the two different protocols could be related to a different reaction pathway. Due to the large amount and high dispersion of Cu in the hydrotalcite materials the TCE is likely to be adsorbed on the Cu phase to a large extent, which is responsible for the cleavage of the C–Cl bond, producing a dechlorinated product. It is well known that copper is an extremely good metal for C–Cl bond cleavage, with dehalogenation occurring even at very low temperatures [37]. However, Cu shows a poor ability for hydrogen chemisorption to create H atoms which can be utilized in cleaning the Cl–Cu surface by formation of HCl. Consequently, the addition of a noble metal capable to hydrogen chemisorption is needed. Furthermore, noble metals are very efficient for the hydrodehalogenation of chlorocompounds to produce deep hydrogenation products [38]. The participation of spillover hydrogen in catalytic hydrodechlorination reactions has already been reported elsewhere [39–42], e.g. for hydrodechlorination of chlorobenzenes on Ni/SiO_2 [42], on Pd supported on carbon [40] and nickel phosphide on SiO_2 catalysts [39,41].

For the catalysts prepared using the first protocol, showing alloy formation between noble metal and copper, copper is responsible for the dehalogenation of TCE to ethylene, whereas the noble metal–copper alloy is responsible for providing hydrogen for the regeneration of the Cu–Cl_x surface by forming HCl species. Due to the presence of the alloy, the noble metal is not able to perform the full hydrogenation of the olefin obtaining a catalyst with a high selectivity to ethene. For the catalysts using the second protocol, showing separate copper and noble metal phases, the selectivity toward ethene is also high at short reaction time but decreases with time on stream. At the beginning of the reaction both the copper and the noble metal are active. On Cu, which is in large excess and possesses a high initial activity (see Fig. 7), ethene is formed as the main product. However, during the reaction the copper surface is poisoned by chloride species and ethane is formed on the noble metal as the main product. Probably, the less effective regeneration of the Cu–Cl_x species on the surface of the catalysts consisting of separate Cu and noble metal particles could explain this catalytic behavior.

To test this assumption we carried out the following experiment (see Fig. 10): the 0.5% Pt-$Mg_{1.5}Cu_{1.5}Al_1$-WR catalyst, after three hours on stream, was reactivated for two hours in hydrogen/helium mixture without the presence of TCE. During this process HCl species were probably removed from the surface of the catalyst. Then, the reaction was started again. Fig. 10 shows that after this cleaning procedure the selectivity returns to the initial values, with ethene as the main product, and then starts going down again, supporting our hypothesis.

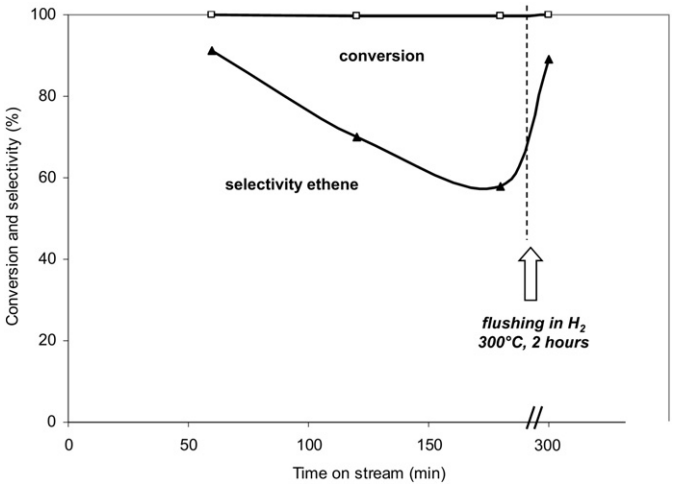

Fig. 10. Conversion and selectivity to ethene on 0.5% Pt-$Mg_{1.5}Cu_{1.5}Al_1$-WR at 300 °C (molar ratio H_2:TCE = 3:1). After 3 h time on stream flushing with H_2/He for 2 h and then switching back to the reaction mixture. (□, TCE conversion; ▲, ethene selectivity.)

4. Conclusions

Pt, Pd-Cu-hydrotalcite catalysts were prepared using different synthesis protocols. HRTEM measurements of the materials prepared by the two different protocols revealed fundamental differences at the microstructural level. Cu–noble metal alloy formation was found on the samples prepared with a reduction step before Pd (Pt) introduction, whereas no alloy formation and the occurrence of separate Pd (Pt) and Cu particles was observed on the samples prepared without reduction step during synthesis. These catalytic materials showed high activity and selectivity to ethene in the hydrodechlorination reaction of TCE. At the reaction temperature of 300 °C and stoichiometric conditions of H_2/TCE, high conversion (>90%) and excellent selectivity toward ethene (>90%) were obtained.

Hardly any influence of the Mg:Cu ratio both on activity and selectivity of the obtained catalysts was observed. However, a strong influence on the selectivity to ethene during time on stream was observed when changing the synthesis protocol of the Pt, Pd-Cu-hydrotalcite catalysts.

Changing the preparation procedure, performing a reduction step before introducing the noble metal ("-R") or without this preceding step ("-WR"), led to a different selectivity to ethene. The interaction between copper with the noble metal forming an alloy or forming separate Cu and noble metal phases is the key to control the selectivity to ethene.

A reaction scheme that involves adsorption of TCE on the Cu phase leading to dechlorination reaction producing ethene is proposed. The main role of the noble metal forming the alloy is the regeneration of the Cu–Cl_x species by spillover of hydrogen. On the alloyed particles a high selectivity to ethene is obtained. However, on catalysts containing copper and the noble metal in separate form the dehalogenation reaction occurs on the copper surface whereas on the surface of the noble metal a deep hydrogenation to ethane is taking place.

Since the role of the noble metal is mainly activation of hydrogen for regeneration of copper or deep hydrogenation of the chlorocompound, we did not observe a significant influence of the nature of the noble metal component.

Acknowledgments

This work was financially supported by the Ministerio de Educación y Ciencia of Spain (CTQ2006-08196, HU2006-0026 and ENE2006-06925), by the Austrian exchange service (Acciones Integradas, ES 05/2007) and the Hochschuljubiläumsstiftung (Gemeinde Wien, Project H-979/2004).

References

[1] S. Ordonez, F.V. Diez, H. Sastre, Ind. Eng. Chem. Res. 41 (2002) 505.
[2] C.G. Schreier, M. Reinhard, Chemosphere 31 (1995) 3475.
[3] S. Ordonez, H. Sastre, F.V. Diez, Appl. Catal. B Environ. 25 (2000) 49.
[4] S. Lambert, F. Ferauche, A. Brasseur, J.P. Pirard, B. Heinrichs, Catal. Today 100 (2005) 283.
[5] V.I. Kovalchuk, J.L. d'Itri, Appl. Catal. A Gen. 271 (2004) 13.
[6] V.Y. Borovkov, D.R. Luebke, V.I. Kovalchuk, J.L. d'Itri, J. Phys. Chem. B 107 (2003) 5568.
[7] W.D. Rhodes, K. Lazar, V.I. Kovalchuk, J.L. d'Itri, J. Catal. 211 (2002) 173.
[8] B. Heinrichs, F. Noville, J.P. Schoebrechts, J.P. Pirard, J. Catal. 220 (2003) 215.
[9] S. Jujjuri, E. Ding, S.G. Shore, M.A. Keane, J. Mol. Catal. A Chem. 272 (2007) 96.
[10] A. Srebowata, W. Juszczyk, Z. Kaszkur, J.W. Sobczak, L. Kepinski, Z. Karpinski, Appl. Catal. A Gen. 319 (2007) 181.
[11] N.C. Concibido, T. Okuda, W. Nishijima, M. Okada, Appl. Catal. B Environ. 71 (2007) 64.
[12] B. Coq, F. Medina, D. Tichit, A. Morato, Catal. Today 88 (2004) 127.
[13] B. Coq, G. Ferrat, F. Figueras, J. Catal. 101 (1986) 434.
[14] S. Ordonez, H. Sastre, F.V. Diez, Appl. Catal. B Environ. 29 (2001) 263.
[15] A. Morato, C. Alonso, F. Medina, Y. Cesteros, P. Salagre, J.E. Sueiras, D. Tichit, B. Coq, Appl. Catal. B Environ. 32 (2001) 167.
[16] S. Ordonez, H. Sastre, F.V. Diez, Appl. Catal. B Environ. 40 (2003) 119.
[17] B. Coq, J.M. Cognion, F. Figueras, D. Tournigant, J. Catal. 141 (1993) 21.
[18] M. Crivello, C. Perez, E. Herrero, G. Ghione, S. Casuscelli, E. Rodriguez-Castellon, Catal. Today 107–108 (2005) 215.
[19] S. Kannan, A. Dubey, H. Knözinger, J. Catal. 231 (2005) 381.
[20] P. Kim, H. Kim, J.B. Joo, W. Kim, I.K. Song, J. Yi, J. Mol. Catal. A Chem. 256 (2006) 178.
[21] A. Alejandre, F. Medina, P. Salagre, X. Correig, J.E. Sueiras, Chem. Mater. 11 (1999) 939.
[22] A. Alejandre, F. Medina, X. Rodriguez, P. Salagre, J.E. Sueiras, J. Catal. 188 (1999) 311.
[23] B.T. Meshesha, R.J. Chimentao, F. Medina, J.E. Sueiras, Y. Cesteros, P. Salagre, F. Figueras, Appl. Catal. B Environ. (2008), doi:10.1016/j.apcatb.2008.08.012, in press.
[24] D. Tichit, B. Coq, Cattech 7 (2003) 206.
[25] F. Kovanda, K. Jiratova, J. Rymes, D. Kolousek, Appl. Clay Sci. 18 (2001) 71.
[26] I.J. Shannon, F. Rey, G. Sankar, J.M. Thomas, T. Maschmeyer, A.M. Waller, A.E. Palomares, A. Corma, A.J. Dent, G.N. Greaves, J. Chem. Soc. Faraday Trans. 92 (1996) 4331.
[27] S. Kannan, V. Rives, H. Knözinger, J. Solid State Chem. 177 (2004) 319.
[28] W.P. Dow, Y.P. Wang, T.J. Huang, Appl. Catal. A Gen. 190 (2000) 25.
[29] K.I. Hadjiivanov, G.N. Vayssilov, Adv. Catal. 47 (2002) 307.
[30] A.A. Davydov, Infrared Spectroscopy of Adsorbed Species on the Surface of Transition Metal Oxides, Wiley, Chichester, 1990.
[31] S.C. Fung, J.H. Sinfelt, J. Catal. 103 (1987) 220.
[32] M. Legawiec-Jarzyna, A. Srebowata, W. Juszczyk, Z. Karpinski, Appl. Catal. A Gen. 271 (2004) 61.
[33] A. Wiersma, E.J.A.X. van de Sandt, M.A. den Hollander, H. van Bekkum, M. Makkee, J.A. Moulijn, J. Catal. 177 (1998) 29.
[34] V. Dal Santo, C. Dossi, S. Recchia, P.E. Colavita, G. Vlaic, R. Psaro, J. Mol. Catal. A Chem. 182/183 (2002) 157.
[35] L.S. Vadlamannati, D.R. Luebke, V.I. Kovalchuk, J.L. d'Itri, Stud. Surf. Sci. Catal. A 130 (2000) 233.
[36] B. Heinrichs, J.P. Schoebrechts, J.P. Pirard, J. Catal. 200 (2001) 309.
[37] Y. Jugnet, J.C. Bertolini, L.A.M.M. Barbosa, P. Sautet, Surf. Sci. 505 (2002) 153.
[38] J.W. Bae, J.S. Lee, K.H. Lee, Appl. Catal. A Gen. 334 (2008) 156.
[39] X. Liu, J. Chen, J. Zhang, Ind. Eng. Chem. Res. 47 (2008) 5362.
[40] C. Amorim, M.A. Keane, J. Colloid Interface Sci. 322 (2008) 196.
[41] X. Liu, J. Chen, J. Zhang, Catal. Commun. 8 (2007) 1905.
[42] M.A. Keane, G. Tavoularis, React. Kinet. Catal. Lett. 78 (2003) 11.